Table 2. Biochemical Parameters and Coronary Artery Calcification During the Study

	Sevelamer (n = 91)				Calcium Carbonate (n = 92)					
Variable	Baseline	Final	Mean Change (95% CI)	*P*	Baseline	Final	Mean Change (95% CI)	*P*	Difference in Mean Change (95% CI)	*P*[a]
Albumin (g/dL)	4.03 ± 0.42	3.92 ± 0.37	−0.10 (−0.17 to −0.04)	0.001	4.03 ± 0.42	3.91 ± 0.40	−0.12 (−0.20 to −0.05)	0.002	0.02 (−0.08 to 0.12)	0.7
Calcium corrected (mg/dL)	9.79 ± 0.79	9.61 ± 0.60	−0.18 (−0.33 to −0.03)	0.02	9.71 ± 0.63	9.85 ± 0.79	0.14 (−0.003 to 0.28)	0.06	−0.32 (−0.52 to −0.12)	0.002
Phosphorus (mg/dL)	5.65 ± 0.56	5.15 ± 0.83	−0.50 (−0.69 to −0.31)	<0.001	5.75 ± 0.76	5.14 ± 0.94	−0.61 (−0.81 to −0.41)	<0.001	0.11 (−0.17 to 0.38)	0.7
Ca × P (mg^2/dL^2)	55.33 ± 7.10	49.50 ± 8.71	−5.83 (−7.73 to −3.92)	<0.001	55.78 ± 7.8	50.56 ± 9.8	−5.21 (−7.23 to −3.20)	<0.001	−0.62 (−3.37 to 2.14)	0.5
Intact PTH (pg/mL)	235.6 ± 169.9	233.9 ± 196.4	−1.7 (−44.5 to 41.2)	0.9	214.9 ± 137.3	237.5 ± 231.8	22.6 (−16.0 to 61.1)	0.2	−24.2 (−38.9 to 42.2)	0.5
LDL-C (mg/dL)	92.1 ± 25.6	72.9 ± 27.7	−19.2 (−24.6 to −13.8)	<0.001	97.2 ± 33.2	98.9 ± 33.1	1.6 (−3.5 to 6.8)	0.5	−20.8 (−28.2 to −13.4)	<0.001
HDL-C (mg/dL)	50.8 ± 14.4	50.4 ± 18.2	−0.4 (−2.6 to 1.9)	0.7	51.2 ± 17.6	51.0 ± 17.7	−0.2 (−3.1 to 2.7)	0.9	−0.2 (−3.8 to 3.5)	0.9
Pentosidine (nmol/mL)	1.861 ± 0.761	1.882 ± 0.860	0.022 (−0.072 to 0.116)	0.6	1.845 ± 0.907	2.121 ± 0.930	0.276 (0.167 to 0.385)	<0.001	−0.254 (−0.396 to −0.112)	<0.001
WBC (/μL)	5,373 ± 1,557	5,295 ± 1,508	−78 (−322 to 166)	0.5	5,548 ± 2,070	5,421 ± 1,704	−127 (−370 to 116)	0.3	49 (−293 to 391)	0.9
CACS	879 ± 1,334	961 ± 1,438	81.8 (42.9 to 120.6)	<0.001	872 ± 1,186	1,066 ± 1,380	194.0 (139.7 to 248.4)	<0.001	−112.3 (−178.8 to −45.8)	<0.001

Note: Continuous variables are expressed as mean ± standard deviation and compared using paired *t* test. Difference in mean change represents the difference between the sevelamer and calcium-carbonate groups in the mean value of change from baseline. The difference between groups was analyzed using ANCOVA after controlling for baseline values, and the obtained *P* values are presented in the far right column. Conversion factors for units: albumin in g/dL to g/L, ×10; calcium in mg/dL to mmol/L, ×0.2495; phosphorus in mg/dL to mmol/L, ×0.3229; LDL-C and HDL-C in mg/dL to mmol/L, ×0.02586; no conversion necessary for PTH in pg/mL and ng/L and pentosidine in nmol/L and mmol/L.

Abbreviations: ANCOVA, analysis of covariance; CACS, coronary artery calcification score; Ca × P, calcium-phosphorus product; CI, confidence interval; HDL-C, high-density lipoprotein cholesterol; LDL-C, low-density lipoprotein cholesterol; PTH, parathyroid hormone; WBC, white blood cell count.

[a]ANCOVA.

treated participants, 72 received sevelamer alone and 7 received sevelamer and calcium carbonate. All participants in the calcium-carbonate arm received calcium carbonate only. Adverse events were constipation (n = 2) in the sevelamer arm and persistent increases in serum calcium levels (>11 mg/dL; n = 5) in the calcium-carbonate arm.

The 2 groups were similar in baseline characteristics (Table 1). Coronary artery disease at study entry included previous myocardial infarction, history of coronary angioplasty and/or stent placement, angina pectoris, evidence of coronary atherosclerotic disease, stroke, transient ischemic attack, and claudication. Phosphate-binder use before study entry included monotherapy with sevelamer or calcium carbonate, their combination, and other phosphate-binder combinations, such as calcium carbonate and calcium acetate.

Coronary Artery Calcification

At baseline, 10 (11.6%) and 8 (9.7%) participants in the sevelamer and calcium-carbonate arms had no detectable coronary artery calcification, respectively. During the 12-month treatment, absolute values for CACS increased significantly in both groups ($P < 0.001$; Table 2). Analysis of covariance after adjusting for baseline values showed that the mean change in CACS was significantly smaller for the sevelamer group ($P < 0.001$; Table 2). The proportion of participants with a ≥15% increase in CACS also was significantly smaller for the sevelamer group ($P = 0.002$; Table 3; Fig 2), with a ≥15% increase in CACS in 35% of the sevelamer group and 59% of the calcium-carbonate group.

Biochemical Parameters

Baseline biochemical parameters were not different between the groups at study entry (Table 2). During treatment, serum albumin levels decreased significantly in both groups ($P = 0.001$ for the sevelamer and $P = 0.002$ for the calcium-carbonate groups). Serum calcium levels showed no significant change in either group (Table 2), whereas values at study completion were significantly higher for the calcium-carbonate group ($P = 0.002$; Table 2; Fig 3). Serum phosphorus and calcium-phosphorus product values decreased from baseline in both groups ($P < 0.001$; Table 2) and were indistinguishable at study completion between groups (Table 2; Fig 3). PTH and high-density lipoprotein cholesterol levels were unchanged in both groups. LDL cholesterol levels decreased significantly in only the sevelamer group ($P < 0.001$) and were significantly lower for the sevelamer group at study completion ($P < 0.001$; Table 2). Plasma pentosidine levels increased in only the calcium carbonate group ($P < 0.001$; Table 2; Fig 4), and analysis of covariance after adjusting for baseline values showed that plasma pentosidine levels were significantly higher in the sevelamer group at completion of treatment ($P < 0.001$).

Table 3. Treatment Effect on CAC Progression in Subgroups Defined by Baseline Variables

	No.	OR (95% CI) for ≥15% Increase in CACS	P
Intervention effect			
Calcium carbonate	92	1.00 (reference)	
Sevelamer	91	0.38 (0.21-0.69)	0.002
Interaction between intervention and each variable			
Sex	183	NA	0.5
Age (y)	183	NA	0.3
HD vintage (mo)	183	NA	0.3
Diabetes mellitus	183	NA	0.3
Baseline Ca × P (mg^2/dL^2)	183	NA	0.7
Baseline LDL cholesterol	183	NA	0.5
Baseline pentosidine	183	NA	0.1
Baseline CACS	183	NA	0.8

Note: ORs for a ≥15% increase from baseline CACS were determined for the sevelamer and calcium-carbonate groups, and that for the sevelamer group is presented using as reference the OR for the calcium-carbonate group. Interaction between intervention and each variable was determined, and *P* value is presented for each variable.

Abbreviations: CAC, coronary artery calcification; CACS, coronary artery calcification score; Ca × P, calcium-phosphorus product; CI, confidence interval; HD, hemodialysis; LDL, low-density lipoprotein; NA, not applicable; OR, odds ratio.

During the course of the study, suppression of PTH (<150 pg/mL) occurred at similar frequencies (38.0% and 40.5% in the sevelamer and calcium-carbonate groups, respectively; not significant). Increases in LDL cholesterol levels (>120 mg/dL) were more frequent in the calcium-carbonate group (20.2% vs 15.2%; $P = 0.001$).

Treatment Effect Interacted With Each Variable on CACS Progression

The treatment effect on the risk of a ≥15% increase in CACS was analyzed using logistic regression. Compared with calcium carbonate, sevelamer therapy was associated with decreased risk of a ≥15% increase in CACS (Table 3). We also evaluated effect modification using cross-product terms (interaction terms) in the model to test the relationship between intervention and each variable (sex, age, HD vintage, presence or absence of diabetes mellitus, baseline LDL cholesterol level, baseline pentosidine level, baseline CACS, or baseline calcium-phosphorus product). There were no statistically significant interactions (Table 3).

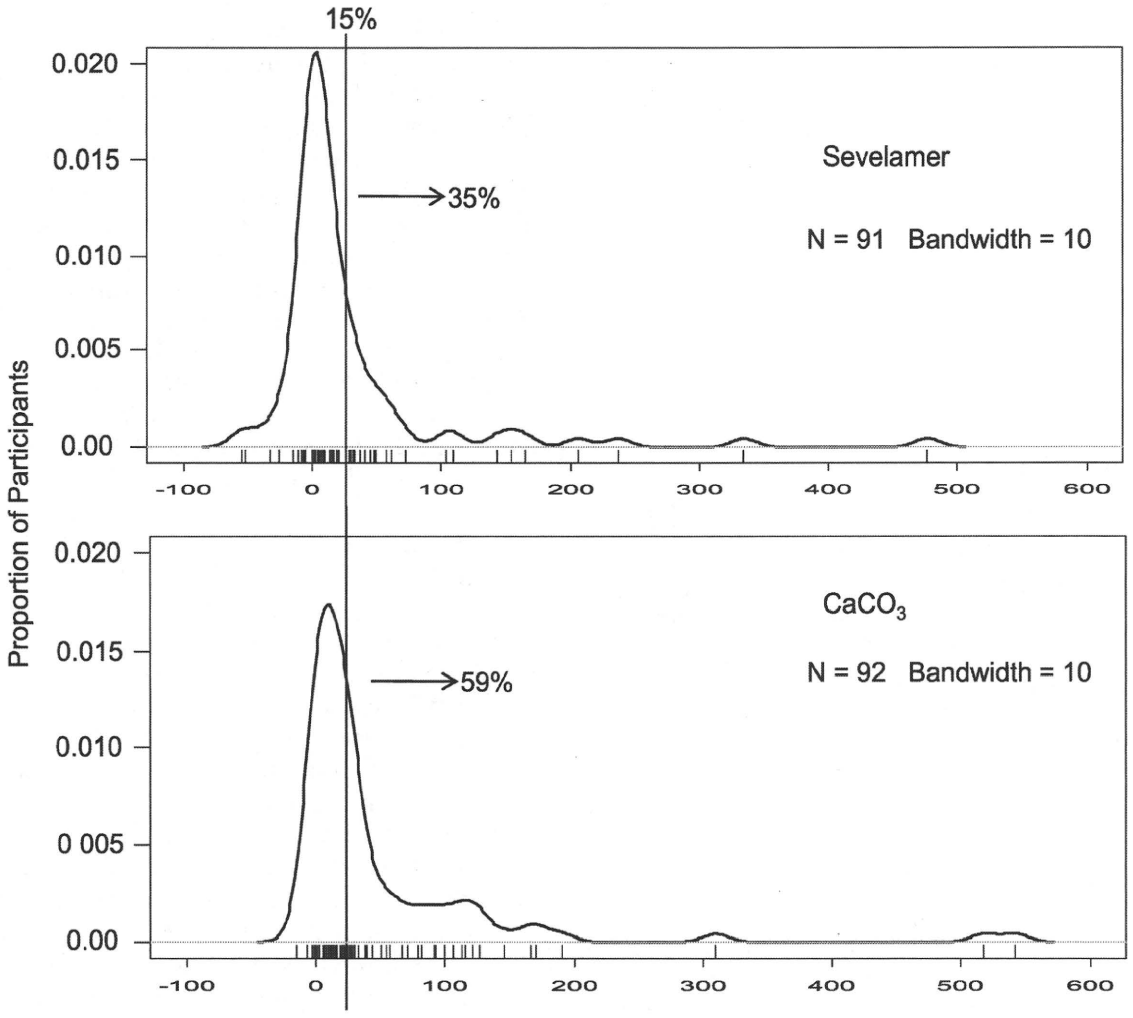

Figure 2. Distribution of participants according to percentage of increase from baseline coronary artery calcification score (CACS). The vertical line represents a 15% increase in CACS. The percentage of participants with a ≥15% increase in CACS is indicated for each group. Abbreviation: $CaCO_3$, calcium carbonate.

DISCUSSION

This randomized trial showed that sevelamer and calcium carbonate were equipotent in decreasing serum phosphorus levels in HD patients, whereas sevelamer resulted in a smaller increase in CACS. Compared with calcium carbonate, sevelamer was associated with decreased risk of progression of coronary artery calcification regardless of sex, age, HD vintage, CACS, and levels of serum calcium and phosphorus, LDL cholesterol, and plasma pentosidine at baseline.

For the study duration of 12 months, the increases of 211 (95% confidence interval, 153-270) and 90 (95% confidence interval, 45-134) in CACS with calcium carbonate and sevelamer, respectively, are similar to the corresponding values of 484 and 37 in a 21-month trial,[30] 37 and 0 in a 52-week trial,[26] and 42 and 0 in an 18-month trial.[29] It deserves mention that dialysis vintages of the present participants, 107 ± 86 and 119 ± 94 months for the sevelamer and calcium-carbonate arms, respectively, are longer than the 68 ± 64 and 55 ± 64 months in Asmus et al,[30] 69 ± 65 and 58 ± 66 months in Braun et al,[28] and median vintage of 3.6 and 2.9 years in Chertow et al.[26] Thus, our trial extends the previously described beneficial effect of sevelamer on coronary artery calcification to HD patients with a relatively longer vintage.

Sevelamer and calcium-carbonate therapy decreased serum phosphorus levels, with no significant change in PTH levels. Serum calcium levels showed a statistically insignificant increase and decrease with calcium carbonate and sevelamer, respectively, resulting in a significant difference between groups at study completion. Sevelamer was associated with decreased risk of progression of coronary artery calcification regardless of baseline serum calcium concentration. Seminal in warning against calcium-based phosphate binder–associated calcium intake were reports that

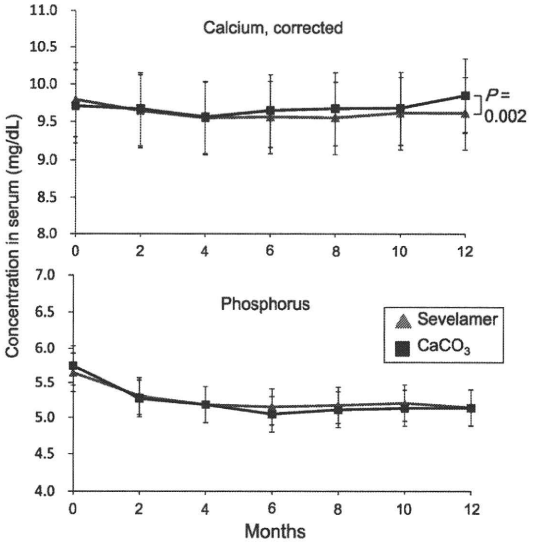

Figure 3. Changes in serum calcium and phosphorus concentrations during treatment. Serum calcium and phosphorus concentrations were determined at study entry and every 2 weeks thereafter during treatment. Values are mean ± standard deviation. Conversion factors for units: phosphorus in mg/dL to mmol/L, ×0.3229; calcium in mg/mL to mmol/L, ×0.2495. Abbreviation: $CaCO_3$, calcium carbonate.

dialysis patients with coronary artery calcification had higher calcium intake than those without,[2] and calcium-based phosphate-binder dose correlated positively with severity of arterial calcification.[7,21] Calcium-based phosphate binders were more likely than sevelamer to cause low PTH level episodes, hypercalcemia,[26,29,43] and decreased trabecular bone density.[30] Our trial had more withdrawals for increased serum calcium levels in the calcium-carbonate arm, indicating the occurrence of calcium loading. However, in the present patients who completed the study without hypercalcemic events, serum calcium levels had no influence on the effect of sevelamer on the progression of coronary artery calcification. Moreover, both binders resulted in similar incidences of low PTH levels and no significant changes in PTH levels. Thus, given that dialysate concentration was the same and dietary calcium intake was not controlled in the present trial, calcium loading with calcium carbonate had a minor role in the difference observed in the effect on coronary artery calcification, except when so extreme to have precipitated hypercalcemia.

Only sevelamer decreased LDL cholesterol levels, whereas calcium carbonate resulted in more frequent increases in LDL cholesterol levels (>120 mg/dL). Sevelamer's effect on the risk of progression of coronary artery calcification was not affected by baseline LDL cholesterol level. Decreases in LDL cholesterol levels commonly occur with sevelamer use[26,29,43,44] and are explained because sevelamer shares the cationic character of bile acid sequestrants[45,46] and has a cooperative high-capacity bile acid–binding ability.[47] The potential of lipid-lowering therapy on vascular calcification was suggested first by the report that statins decreased the volume of calcified plaques in coronary arteries.[48] Lipid-lowering therapy attenuated the progression of coronary artery calcification in patients with LDL cholesterol levels >130 mg/dL[49] and hypercholesterolemic postmenopausal women.[50] However, a recent trial showed that halving LDL cholesterol levels using statins had no effect on the progression of coronary artery calcification.[51] In the trials of sevelamer, the associations between coronary artery calcification and LDL cholesterol level were unsubstantiated,[26] not significant,[4,43] or inconclusive.[29] The benefit of lipid-lowering therapy in general was documented when participants had mean LDL cholesterol levels ≥120,[48] >130,[49] or 175.3 ± 32.4 mg/dL.[50] It is possible that the number of patients with baseline LDL cholesterol levels ≥120 mg/dL in the present study was too small to assess the clinical significance of the LDL cholesterol-lowering effect of sevelamer.

Plasma pentosidine levels increased in only the calcium-carbonate group and were significantly higher in the calcium-carbonate group at study completion. Sevelamer therapy was associated with decreased risk of progression of coronary artery calcification regardless of baseline plasma pentosidine concentration. Pentosidine is a representative AGE often used as a marker for AGEs.[52,53] Initially believed to occur only under a high carbohydrate milieu, pentosidine and other AGEs are present in nondiabetic uremic patients in concentrations higher than those in diabetic patients.[40,54-58] Formation of pentosidine and N^{ϵ}(carboxyl-methyl)lysine, an AGE structure, in uremia is driven by accumulating reactive carbonyl compounds,[53,59] which are generated not only from carbohydrates but also from polyunsaturated fatty acids

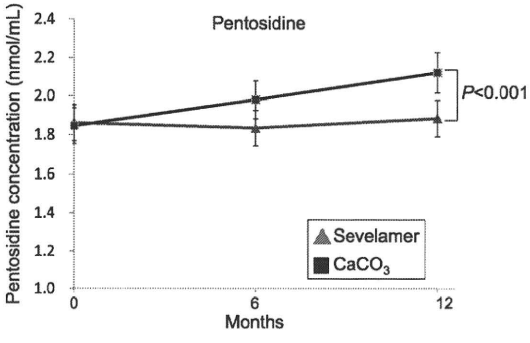

Figure 4. Changes in plasma pentosidine concentrations during treatment. Plasma pentosidine concentrations were determined at study entry, 6 months into the treatment, and study completion, and the mean of each determination is presented. No conversion necessary for pentosidine in nmol/mL and mmol/L. Abbreviation: $CaCO_3$, calcium carbonate.

through peroxidation[60] and modify proteins to form advanced lipoxidation end products.[53] Levels of these products also are increased in uremia.[53,61-63] A link was presented for AGEs and vascular calcification when increased plasma pentosidine levels were correlated with severity of abdominal aorta calcification in HD patients.[37] Taki et al[38] determined levels of circulating pentosidine, N^{ϵ}(carboxyl-methyl)lysine, malondialdehyde, and lipid peroxides along with traditional cardiovascular risk factors and calcium overload in HD patients and concluded that AGEs and oxidative stress were associated with coronary artery calcification independent of previously described risk factors. An 18-year follow-up also showed a significant correlation between increased circulating AGE levels and increased cardiovascular and coronary disease mortality in nondiabetic women.[64] Thus, the present prospective trial provided further evidence for the association between AGE accumulation and progression of coronary artery calcification. However, analysis after controlling for pentosidine level change from baseline as a covariate produced $P = 0.661$ for pentosidine level and $P = 0.001$ for intervention, indicating that the effect of the intervention is not mediated by the change in pentosidine levels. It is possible that calcium-based phosphate binder–associated calcium loading entails AGE accumulation, resulting in enhanced coronary artery calcification.

Multiple lines of evidence indicate that AGEs and oxidative stress are involved in the pathogenesis of cardiovascular disease.[34,65-67] Notably, atherogenesis and vascular calcification were enhanced by uremia in apolipoprotein E–deficient mice[68-70] and attenuated by oral sevelamer therapy, with decreases in serum phosphorus and PTH levels and oxidative damage, whereas levels of serum total cholesterol, calcium, and uremic toxins were unaffected,[71] suggesting a relationship between AGEs and the effect of sevelamer on vascular calcification in uremia. However, because the contribution of dietary AGEs to their plasma levels has been documented,[72-74] we cannot deny the possibility that sevelamer decreased appetite and dietary AGE intake, resulting in decreased plasma pentosidine levels.

Limitations of the present study were that treatment duration was relatively short, treatment was open label, some sevelamer-treated participants (7 of 79) also received calcium carbonate, and statistical power was 80%. Washout could not be performed because participants were well informed of the risk of hyperphosphatemia and were unwilling to discontinue phosphate-binder therapy.

In conclusion, our findings extended the beneficial effect of sevelamer to HD patients with relatively long vintage and suggested a relationship between the effect of sevelamer on the progression of coronary artery calcification and suppression of AGE accumulation.

ACKNOWLEDGEMENTS

This study was presented in part at the 40th Congress of the American Society of Nephrology, San Francisco, CA, October 31-November 5, 2007.

We thank Mrs Hiroko Yuzawa and Mr Shu Ikeda for determination of pentosidine levels and CACS, respectively; Mr Mitsuhiro Isozaki for statistical analysis; Dr Teiryo Maeda for advice on study design; and Dr Toshio Homma for editorial assistance.

Support: This study was supported in part by grants from the Japan Dialysis Outcomes Research Group.

Financial Disclosure: The authors declare that they have no relevant financial interests.

REFERENCES

1. Braun J, Oldendorf M, Moshage W, Heidler R, Zeitler E, Luft FC. Electron beam computed tomography in the evaluation of cardiac calcification in chronic dialysis patients. *Am J Kidney Dis.* 1996;27:394-401.

2. Goodman WG, Goldin J, Kuizon BD, et al. Coronary-artery calcification in young adults with end-stage renal disease who are undergoing dialysis. *N Engl J Med.* 2000;342:1478-1483.

3. Blacher J, Guerin AP, Pannier B, Marchais SJ, London GM. Arterial calcifications, arterial stiffness, and cardiovascular risk in end-stage renal disease. *Hypertension.* 2001;38:938-942.

4. Raggi P, Boulay A, Chasan-Taber S, et al. Cardiac calcification in adult hemodialysis patients. A link between end-stage renal disase and cardiovascular disease? *J Am Coll Cardiol.* 2002;39:695-701.

5. Blacher J, Guerin A, Pannier B, Marchais S, Safar M, London G. Impact of aortic stiffness on survival in end-stage renal disease. *Circulation.* 1999;99:2434-2439.

6. Wilson PW, Kauppila LI, O'Donnell CJ, et al. Abdominal aortic calcific deposits are an important predictor of vascular morbidity and mortality. *Circulation.* 2001;103:1529-1534.

7. London GM, Guérin AP, Marchais SJ, Métvier F, Pannier B, Adda H. Arterial media calcification in end-stage renal disease: impact on all-cause and cardiovascular mortality. *Nephrol Dial Transplant.* 2003;18:1731-1740.

8. Giachelli CM. Ectopic calcification. Gathering hard facts about soft tissue mineralization. *Am J Pathol.* 1999;154:671-675.

9. Giachelli CM. Vascular calcification mechanisms. *J Am Soc Nephrol.* 2004;15:2959-2964.

10. Shao JS, Cai J, Towler DA. Molecular mechanisms of vascular calcification. Lessons learned from the aorta. *Arterioscler Thromb Vasc Biol.* 2006;26:1423-1430.

11. Moe SM, Chen NX. Mechanisms of vascular calcification in chronic kidney disease. *J Am Soc Nephrol.* 2008;19:213-216.

12. Kimura K, Saika Y, Otani H, Fujii R, Mine M, Yukawa S. Factors associated with calcification of the abdominal aorta in hemodialysis patients. *Kidney Int Suppl.* 1999;71:S238-241.

13. Young EW, Albert JM, Satayathum S, et al. Predictors and consequences of altered mineral metabolism: the Dialysis Outcomes and Practice Patterns Study. *Kidney Int.* 2005;67:1179-1187.

14. Block GA, Hulbert-Shearon TE, Levin NW, Port FK. Association of serum phosphorus and calcium × phosphate product with mortality risk in chronic hemodialysis patients: a national study. *Am J Kidney Dis.* 1998;31:607-617.

15. Block GA, Klassen PS, Lazarus JM, Ofsthun N, Lowrie EG, Chertow GM. Mineral metabolism, mortality, and morbidity

in maintenance hemodialysis. *J Am Soc Nephrol.* 2004;15:2208-2218.

16. Young EW, Akiba T, Albert JM, et al. Magnitude and impact of abnormal mineral metabolism in hemodialysis patients in the Dialysis Outcomes and Practice Patterns Study (DOPPS). *Am J Kidney Dis.* 2004;44:34-38.

17. Stevens LA, Djurdjev O, Cardew S, Cameron EC, Levin A. Calcium, phosphate, and parathyroid hormone levels in combination and as a function of dialysis duration predict mortality: evidence for the complexity of the association between mineral metabolism and outcomes. *J Am Soc Nephrol.* 2004;15:770-779.

18. Jono S, McKee MD, Murry CE, et al. Phosphate regulation of vascular smooth muscle cell calcification. *Circ Res.* 2000;87: e10-17.

19. Reynolds JL, Joannides AJ, Skepper JN, et al. Human vascular smooth muscle cells undergo vesicle-mediated calcification in response to changes in extracellular calcium and phosphate concentrations: a potential mechanism for accelerated vascular calcification in ESRD. *J Am Soc Nephrol.* 2004;15:2857-2867.

20. Lomashvili KA, Cobbs S, Hennigar RA, Hardcastle KI, O'Neill WC. Phosphate-induced vascular calcification: role of pyrophosphate and osteopontin. *J Am Soc Nephrol.* 2004;15:1392-1401.

21. Guérin AP, London GM, Marchais SJ, Métvier F. Arterial stiffening and vascular calcifications in end-stage renal disease. *Nephrol Dial Transplant.* 2000;15:1014-1021.

22. Drueke TB, Touam M. Calcium balance in haemodialysis—do not lower the dialysate calcium concentration too much (con part). *Nephrol Dial Transplant.* 2009;24:2990-2993.

23. Gotch FA. Pro/con debate: the calculation on calcium balance in dialysis lowers the dialysate calcium concentrations (pro part). *Nephrol Dial Transplant.* 2009;24:2994-2996.

24. Chertow GM, Burke SK, Dillon MA, Slatopolsky E; for the RenaGel Study Group. Long-term effects of sevelamer hydrochloride on the calcium × phosphate product and lipid profile of haemodialysis patients. *Nephrol Dial Transplant.* 1999;14:2907-2914.

25. Slatopolsky EA, Burke SK, Dillon A; RenaGel® Study Group. RenaGel®, a nonabsorbed calcium- and aluminum-free phosphate binder, lowers serum phosphorus and parathyroid hormone. *Kidney Int.*1999;55:299-307.

26. Chertow GM, Burke SK, Raggi P; for the Treat to Goal Working Group. Sevelamer attenuates the progression of coronary and aortic calcification in hemodialysis patients. *Kidney Int.* 2002; 62:245-252.

27. Chertow GM, Raggi P, McCarthy JT, et al. The effects of sevelamer and calcium acetate on proxies of atherosclerotic and arteriosclerotic vascular disease in hemodialysis patients. *Am J Nephrol.* 2003;23:307-314.

28. Braun J, Asmus HG, Holzer H, et al. Long-term comparison of a calcium-free phosphate binder and calcium carbonate–phosphorus metabolism and cardiovascular calcification. *Clin Nephrol.* 2004;62:104-115.

29. Block GA, Spiegel DM, Ehrlich J, et al. Effects of sevelamer and calcium on coronary artery calcification in patients new to hemodialysis. *Kidney Int.* 2005;68:1815-1824.

30. Asmus HG, Braun J, Krause R, et al. Two year comparison of sevelamer and calcium carbonate effects on cardiovascular calcification and bone density. *Nephrol Dial Transplant.* 2005; 20:1653-1661.

31. Russo D, Miranda I, Ruocco C, et al. The progression of coronary artery calcification in predialysis patients on calcium carbonate or sevelamer. *Kidney Int.* 2007;72:1255-1261.

32. Block GA, Raggi P, Bellasi A, Kooienga L, Spiegel DM. Mortality effect of coronary artery calcification and phosphate binder choice in incident hemodialysis patients. *Kidney Int.* 2007;71:438-441.

33. Peppa M, Raptis SA. Advanced glycation end products and cardiovascular disease. *Curr Diabetes Rev.* 2008;4:1-9.

34. Himmelfalb J, Stenvinkel P, Ikizler TA, Hakim RM. The elephant in uremia: oxidant stress as a unifying concept of cardiovascular disease in uremia. *Kidney Int.* 2002;62:1524-1538.

35. Locatelli F, Canaud B, Eckardt KU, Stenvinkel P, Wanner C, Zoccali C. Oxidative stress in end-stage renal disease: an emerging threat to patient outcome. *Nephrol Dial Transplant.* 2003;18:1272-1280.

36. Vaziri ND. Oxidative stress in uremia: nature, mechanisms, and potential consequences. *Semin Nephrol.* 2004;24:469-473.

37. Kitauchi T, Yoshida K, Yoneda T, et al. Association between pentosidine and arteriosclerosis in patients receiving hemodialysis. *Clin Exp Nephrol.* 2004;8:48-53.

38. Taki K, Takayama F, Tsuruta Y, Niwa T. Oxidative stress, advanced glycation end product, and coronary artery calcification in hemodialysis patients. *Kidney Int.* 2006;70:218-224.

39. National Kidney Foundation. K/DOQI Clinical Practice Guidelines for Managing Dyslipidemia in Chronic Kidney Disease. *Am J Kidney Dis.* 2003;41(4 suppl 3):S1-91.

40. Miyata T, Ueda Y, Shinzato T, et al. Accumulation of albumin-linked and free-form pentosidine in the circulation of uremic patients with end-stage renal failure: renal implications in the pathophysiology of pentosidine. *J Am Soc Nephrol.* 1996;7: 1198-1206.

41. Kakuta T, Tanaka R, Satoh Y, et al. Pyridoxamine improves functional, structural, and biochemical alterations of peritoneal membranes in uremic peritoneal dialysis rats. *Kidney Int.* 2005;68; 1326-1336.

42. Agatston AS, Janowitz WR, Hildner FJ, Zusmer NR, Viamonte M Jr, Detrano R. Quantification of coronary artery calcium using ultrafast computed tomography. *J Am Coll Cardiol.* 1990;15: 827-832.

43. Chertow GM, Raggi P, Chasan-Taber S, Bommer J, Holzer H, Burke SK. Determinants of progressive vascular calcification in haemodialysis patients. *Nephrol Dial Transplant.* 2004;19:1489-1496.

44. Burke SK, Slatopolsky EA, Goldberg DI. RenaGel®, a novel calcium- and aluminum-free phosphate binder, inhibits phosphate absorption in normal volunteers. *Nephrol Dial Transplant.*1997;12:1640-1644.

45. Mandeville WH, Goldberg DI. The sequestration of bile acids, a non-absorbed method for cholesterol reduction. A review. *Curr Pharm Des.* 1997;3:15-28.

46. Stedronsky ER. Interaction of bile acids and cholesterol with non-systemic agents having hypocholesterolemic properties. *Biochim Biophys Acta.* 1994;1210:255-287.

47. Braunlin WB, Zhorov E, Guo A, et al. Bile acid binding to sevelamer HCl. *Kidney Int.* 2002;62:611-619.

48. Callister TQ, Raggi P, Cooil B, Lippolis NJ, Russo DJ. Effect of HMG-CoA reductase inhibitors on coronary artery disease as assessed by electron-beam computed tomography. *N Engl J Med.* 1998;339:1972-1978.

49. Achenbach S, Ropers D, Pohle K, et al. Influence of lipid-lowering therapy on the progression of coronary artery calcification. A prospective evaluation. *Circulation.* 2002;106:1077-1082.

50. Raggi P, Davidson M, Callister TQ, et al. Aggressive versus moderate lipid-lowering therapy in hypercholesterolemic postmenopausal women. Beyond Endorsed Lipid Lowering With EBT Scanning (BELLES). *Circulation.* 2005;112:563-571.

51. Houslay ES, Cowell SJ, Prescott RJ, et al. Progressive coronary calcification despite intensive lipid-lowering treatment: a randomized controlled trial. *Heart.* 2006;92:1207-1212.

52. Miyata T, Taneda S, Kawai R, et al. Identification of pentosidine as a native structure for advanced glycation end products in β^2-microglobulin forming amyloid fibrils in patients with dialysis-related amyloidosis. *Proc Natl Acad Sci U S A.* 1996;93:2353-2358.

53. Miyata T, Ueda Y, Yamada Y, et al. Accumulation of carbonyls accelerates the formation of pentosidine, an advanced glycation end product: carbonyl stress in uremia. *J Am Soc Nephrol.* 1998;9:2349-2356.

54. Odetti P, Forgarty J, Sell DR, Monnier VM. Chromatographic quantitation of plasma and erythrocyte pentosidine in diabetic and uremic subjects. *Diabetes.* 1992;41:153-159.

55. Monnier VM, Sell DR, Nagaraj RH, et al. Maillard reaction-mediated molecular damage to extracellular matrix and other tissue proteins in diabetes, aging, and uremia. *Diabetes.* 1992;41: 36-41.

56. Monnier VM, Sell DR, Miyata S, Nagaraj RH, Odetti P, Lapolla A. Advanced Maillard reaction products as markers for tissue damage in diabetes and uraemia: relevance to diabetic nephropathy. *Acta Diabetol.* 1992;29:130-135.

57. Friedlander M, Wu Y, Schulak J, Monnier V, Hricik D. Influence of dialysis modality on plasma and tissue concentrations of pentosidine in patients with end-stage renal disease. *Am J Kidney Dis.* 1995;25:445-451.

58. Friedlander M, Wu Y, Elgawish A, Monnier V. Early and advanced glycosylation end products: kinetics of formation and clearance in peritoneal dialysis. *J Clin Invest.* 1996;97:728-735.

59. Weiss MF, Erhard P, Kader-Attia FA, et al. Mechanisms for the formation of glycoxidation products in end-stage renal disease. *Kidney Int.* 2000;57:2571-2585.

60. Esterbauer H, Schuer RJ, Zollner H. Chemistry and biochemistry of 4-hydroxynonenal, malondialdehyde and related aldehyde. *Free Radic Biol Med.* 1991;11:81-128.

61. Miyata T, Fu MX, Kurokawa K, van Ypersele de Strihou C, Thorpe SR, Baynes JW. Autoxidation products of both carbohydrates and lipids are increased in uremic plasma: is there oxidative stress in uremia? *Kidney Int.* 1998;54:1290-1295.

62. Odani H, Shinzato H, Matsumoto Y, Usami J, Maeda K. Increase in t(ree α, β-dicarbonyl compound levels in human uremic plasma: specific in vivo determination of intermediates in advanced Maillard reaction. *Biochem Biophys Res Commun.* 1999; 256:89-93.

63. Miyata T, van Ypersele de Strihou C, Kurokawa K, Baynes JW. Alterations in non-enzymatic biochemistry in uremia: origin and significance of "carbonyl stress" in long-term uremic complications. *Kidney Int.* 1999;55:389-399.

64. Kilhovd BK, Juutilainen A, Lehto S, et al. High serum levels of advanced glycation end products predicts increased coronary heart disease mortality in nondiabetic women but not in nondiabetic men. A population-based 18-year follow-up study. *Arterioscler Thromb Vasc Biol.* 2005;25:815-820.

65. Schmidt AM, Yan SD, Wautier JL, Stern D. Activation of receptor for advanced glycation end products. A mechanism for chronic vascular dysfunction in diabetic vasculopathy and atherosclerosis. *Circ Res.* 1999;84:489-497.

66. Baynes JW, Thorpe SR. Glycoxidation and lipoxidation in atherogenesis. *Free Radic Biol Med.* 2000;28:1708-1716.

67. Himmelfalb J. Relevance of oxidative pathways in the pathophysiology of chronic kidney disease. *Cardiol Clin.* 2005;23: 319-330.

68. Buzello M, Törnig J, Faulhaber J, Ehmke H, Ritz E, Amann K. The apolipoprotein E knockout mouse: a model documenting accelerated atherogenesis in uremia. *J Am Soc Nephrol.* 2003;14: 311-316.

69. Bro S, Bentzon JF, Falk E, Andersen CB, Olgaard K, Nielsen LB. Chronic renal failure accelerates atherogenesis in apolipoprotein E-deficient mice. *J Am Soc Nephrol.* 2003;14:2466-2474.

70. Massy ZA, Ivanovski O, Nguyen-Khoa T, et al. Uremia accelerates both atherosclerosis and arterial calcification in apolipoprotein E knockout mice. *J Am Soc Nephrol.* 2005;16:109-116.

71. Phan O, Ivanovski O, Nguyen-Khoa T, et al. Sevelamer prevents uremia-enhanced atherosclerosis progression in apolipoprotein E-deficient mice. *Circulation.* 2005;112:2875-2882.

72. Koschinsky T, He CJ, Mitsuhashi T, et al. Orally absorbed reactive glycation products (glycotoxins): an environmental risk factor in diabetic nephropathy. *Proc Natl Acad Sci U S A.* 1997;94: 6474-6479.

73. Uribarri J, Peppa M, Cai W, et al. Dietary glycotoxins correlate with circulating advanced glycation end product levels in renal failure patients. *Am J Kidney Dis.* 2003;42:532-538.

74. Uribarri J, Peppa M, Cai W, et al. Restriction of dietary glycotoxins reduces excessive advanced glycation end products in renal failure patients. *J Am Soc Nephrol.* 2003;14:728-731.

Pathology International

Pathology International 2010; **60**: 720–725 doi:10.1111/j.1440-1827.2010.02590.x

Original Article

Using immunofluorescent digital slide technology to quantify protein expression in archival paraffin-embedded tissue sections

Akinori Hashiguchi,[1] Yoshinori Hashimoto,[2] Hiroshi Suzuki[1] and Michiie Sakamoto[1]

[1]*Department of Pathology, School of Medicine, Keio University, Tokyo and* [2]*System Division, Hamamatsu Photonics K.K., Hamamatsu, Japan*

Molecularly targeted therapies require an adequate assessment of molecular expression in cancer. Immunofluorescent staining is a better method to quantify protein expression than immunohistochemistry (IHC), although the latter is currently used to score human epidermal growth factor receptor 2 (HER2) and steroid receptors. The quantification of signal intensity in IHC is still controversial. The advanced technology of virtual slides permits digitizing a whole slide image of immunofluorescence for a few minutes. We have established fluorescence-based, immunofluorescent quantification digital slides (IQD), a method widely applicable in routine practice. The IQD were made by scanning images of formalin-fixed, paraffin-embedded sections and contained, not only morphological information obtained from hematoxylin-counterstains, but also immunofluorescent signals. Assessing protein expression on IQD was carried out using the original image analysis software and was compared with the IHC score (HER2 and steroid receptors). There was a statistically significant correlation between the IQD and IHC scores. In addition, we compared IQD scores of groups classified by IHC scores. The IHC intermediate-expression groups were not statistically different from the high, or negative-expression groups. Immunofluorescent quantification digital slides may help pathologists to assess molecular expression in cancer tissue, and resolve the issue of scoring the intensity of brown signal on IHC slides.

Key words: diagnostic molecular pathology, immunofluorescent quantification, quantum dots, virtual microscopy

Since the development of molecular targeted therapy for cancer, the quantitative assessment of protein expression in tissue sections has become a daily task for pathologists.[1,2] Although the antigen-antibody interactions in immunohistochemistry (IHC) are conventionally visualized with the 3, 3′-diaminobenzidine (DAB) chromogen, measuring stain intensity and quantifying protein expression in the chromogenic slides can occasionally be difficult. Immunofluorescent staining is suitable for quantifying protein expression,[3] but the staining is not preserved and it provides little information on tissue morphology.

Virtual microscopy is an advanced technology that converts microscopic glass slide images into digital slides. It has been used for telepathology, consultation, education, tissue microarray, etc.[4–7] Recently virtual microscopy has made it possible to preserve whole slide images of immunofluorescence, almost indefinitely.

We attempted to create an immunofluorescent quantification digital slide (IQD), which contained, not only morphological information obtained from hematoxylin-counterstains, but also immunofluorescent signals. Quantum dots have been successfully applied to IQD technology.[8,9] Using IQD, pathologists can identify the context of a protein's expression pattern on the images of hematoxylin stains, as well as quantifying the level of expression by analyzing immunofluorescent images.

MATERIALS AND METHODS

Specimen selection

After a pathological diagnosis paraffin-embedded tissue blocks were obtained from the files of the Department of Pathology, Keio University School of Medicine and Keio University Hospital. Cases of breast carcinoma that were scored as 'negative, score 0', were not selected.

Correspondence: Michiie Sakamoto, MD, PhD, Department of Pathology, School of Medicine, Keio University, 35 Shinanomachi, Shinjuku-ku, Tokyo 160-8582, Japan. Email: msakamot@sc.itc.keio.ac.jp

Received 2 April 2010. Accepted for publication 7 July 2010.

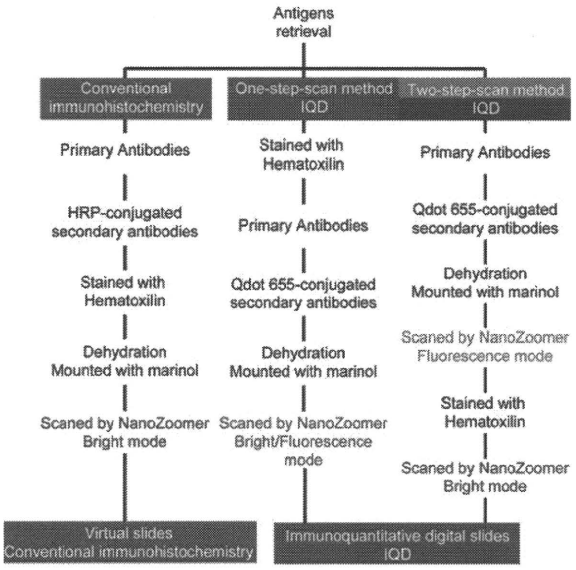

Figure 1 Preparation of immunofluorescent quantification digital slides (IQD). All slides were stained with Mayer's hematoxylin that enables pathologists to observe tissue morphology. Since the hematoxylin chromogen absorbed red emission of Qdot655, when we looked at nuclear antigens hematoxylin staining was carried out after scanning the immunofluorescent images.

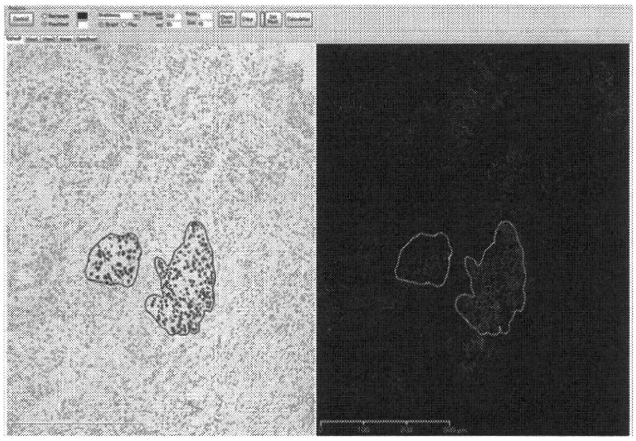

Figure 2 Screen capture of ViewPlus image (human epidermal growth factor receptor 2 [HER2] in breast carcinoma). Immunofluorescent quantification digital slides (IQD) were analyzed by ViewPlus software (Hamamatsu Photonics, Hamamatsu, Japan). Pathologists observed the IQD and selected the area suitable for assessment. The signal intensity in the encircled areas was quantified. The blue coloring represents the nuclei of cancer cells that were semi-automatically detected.

Preparation of IQD

Three-micron thick tissue sections were prepared from the paraffin blocks for immunohistochemistry and immunofluorescence. Sections were deparaffinized, and rehydrated through graded alcohols and distilled water. Heat-induced antigen retrieval was carried out by incubating the slides in 0.01 M citrate buffer (pH 6.0) at 120°C for 20 min. After antigen retrieval, specimens were divided into three groups, as described in Fig. 1. Sections were stained with Mayer's hematoxylin as a nuclear counterstain. Primary antibodies were: anti-CD30, clone Ber-H2 (1:100) (Dako, Glostrup, Denmark); rabbit polyclonal anti-chromogranin A (1:1000) (Dako); anti-c-erbB-2 oncoprotein (HER2), clone CB11 (1:50) (Novocastra, Newcastle upon Tyne, UK); anti-estrogen receptor alpha, clone 1D5 (1:100) (Dako); and anti-progesterone receptor, clone PgR636 (1:100) (Dako); CD3, clone PS1(1:50) (Novocastra); CD20, clone L26 (1:200); CD34, clone QBEnd/10 (1:100) (Novocastra); rabbit polyclonal anti-synaptophysin (1:400) (Dako); Ki-67, clone MIB-1 (1:200) (Dako), TTF-1, clone 8G7G3/1 (1:200) (Dako). Each slide was incubated with secondary antibody according to the manufacturer's protocol. Staining was visualized using the ImmPRESS (Vector Laboratories, Burlingame, CA, USA) peroxidase polymer detection reagents with DAB as the substrate chromogen. We adopted Qdot 655-conjugated secondary antibody (1:100) (Invitrogen, Carlsbad, CA, USA) for the IQD. Qdot 655 was brighter and had a much longer lifetime than organic fluorescent dyes, and its emission peak fell outside the tissue autofluorescence spectrum. After staining, bright and fluorescent imaging of whole slides were obtained with the NanoZoomer (Hamamatsu Photonics, Hamamatsu, Japan). This instrument is able to quickly digitize large areas using time delayed integrated (TDI) sensor technology, and prevents photo-induced deterioration of the fluorescent dyes. To scan the emission of Q-dot655, the IR cut filter, which prevents the color balance from collapsing, was removed from an optical path of the fluorescence.

Immunofluorescent quantification digital slides were established by merging the images of immunofluorescence and hematoxylin staining on exactly the same section. Analyzing the IQD images was carried out using the ViewPlus software (Hamamatsu Photonics).

Quantifying protein expression

The HER2[10] and Allred scores[11] of all the IHC slides were assessed by one pathologist, to avoid inter-observer error. For statistical analysis, the Allred score was further simplified into four categories: negative (Allred 0, 2), or low (Allred 3, 4), medium (Allred 5, 6), and high (Allred 7, 8), as previously described.[12]

To determine the IQD score an adequate area for quantitative analysis was selected by pathologists (Fig. 2). The number of nuclei recognized by the hematoxylin stain was measured as the number of cells. The IQD cell score (HER2, estrogen receptor [ERc] and progesterone receptor [PRc])

was calculated by dividing the sum of its intensity by the number of cells. The IQD intensity score (estrogen receptor [ERi] and progesterone receptor [PRi]) was determined by dividing the sum of the intensity by the total area of the assayed compartment.

Statistical methods

The association of IHC score with IQD was examined using the Spearman's rank correlation coefficient. The IQD scores of the groups classified by IHC scores were compared using one-way ANOVA and the Kruskal-Wallis one-way analysis of variance, and Mann-Whitney tests (a non-parametric test). All *P*-values were two-tailed and values less than 0.05 were considered statistically significant. Since multiple correlations were investigated between the IHC and IQD scores, the *P*-value was adjusted using a Bonferroni correction to allow for the inflation of alpha. Analyses were carried out using SPSS software (version 17.0, SPSS Inc. Chicago, IL, USA).

RESULTS

Establishing IQD

A screen view of IQD is shown in Fig. 3. Immunofluorescent quantification digital slides were able to show images of immunofluorescent and hematoxylin-stained sections simultaneously with 'synchronized' or 'merged' viewing. Initially we captured the immunofluorescent image, then stained with hematoxylin, and re-captured the image (the 'two-step-scan' method as shown in Fig. 1). To skip the first scanning step, we attempted to scan the slides stained with hematoxylin, followed by immunostaining and capturing (the 'one-step-scan' method). The membrane and cytoplasmic antigens that we looked at were CD30, chromogranin, HER2 (Figs 3,4), CD3, CD20, CD34, and synaptophysin (data not shown). Their signal was not significantly disturbed by the hematoxylin, and the localization and intensity of the immunofluorescent signal was almost the same as that with IHC (Fig. 4). On the other hand, signals of nuclear antigens (estrogen and progesterone receptor, Ki-67 and TTF-1 [data not shown]) were significantly diminished, probably because the hematoxylin absorbed red emission from Qdot 655. We attempted other chromogens; methyl green, anyline blue, nuclear fast red, and toluidine blue (data not shown), but hematoxylin staining was the best method to assess nuclear morphology. There was no chromogen compatible with the fluorescent signal of nuclear antigens. Thus, in the case of nuclear antigens, the sections were stained with hematoxylin after capturing the immunofluorescent image (Fig. 1). On serial sections, the stained appearance on the IQD was almost the same as the IHC slides (Fig. 4). Variation in staining intensity, due to fixative and tissue section storage conditions, that was observed in the IHC slides, was also seen in the IQD.

Comparing IQD and IHC scores

To investigate whether IQD could be applied to the quantification of protein expression, we scored the IQD signal, as described above, and compared the IQD scores with those of IHC. The correlation between IQD and IHC scores was analyzed statistically, and the results are shown in Table 1. Each IQD index was calculated, as described in the 'Materials and methods'. The IQD cell index (HER2, ERc and PRc) estimated the amount of the antigen per cell, whereas the IQD intensity index (ERi and PRi) estimated signal intensity. All IQD scores correlated with IHC scores, however the correlation coefficient of ERi and PRi was higher than ERc and PRc. On IHC slides, pathologists were able to assess the signal intensity by color darkness, whereas on IQD they could not only assess signal intensity, but also the amount of antigen per cell.

Comparing the groups classified by the IHC scores was done using the one-way ANOVA and Kruskal-Wallis tests (Fig. 5, Table 1). In the case of estrogen and progesterone receptors, there was no low-expressing group in IHC. There was a statistically significant difference in IQD scores among the IHC groups of ERi, PRc, PRi and HER2, however, there was no significant difference among those of ERc.

Multiple comparisons were investigated between two IHC groups using the Games-Howell test and the Mann-Whitney test with Bonferroni correction.

There was no significant difference between HER2 score 1+ and 2+ (Games-Howell test, *P*-value = 0.60). The PRc scores were not statistically different between 'negative' and 'medium' IHC (Games-Howell test, *P*-value = 0.39). The ERi and PRi scores were different between 'negative' and 'high' IHC (Mann-Whitney test, *P*-value = 0.001 and 0.011). There were no significant differences between 'medium' and other groups (Mann-Whitney test, *P*-value > 0.017).

DISCUSSION

In this study, we show a novel concept for digital slides, applicable to quantifying the molecules in tissue sections. Immunofluorescence has been a useful method for assessing antigen localization and quantifying protein expression in tissue.[3] When applying this method to diagnostic pathology, there are a few difficulties. One problem is the confounding presence of background tissue autofluorescence, which is

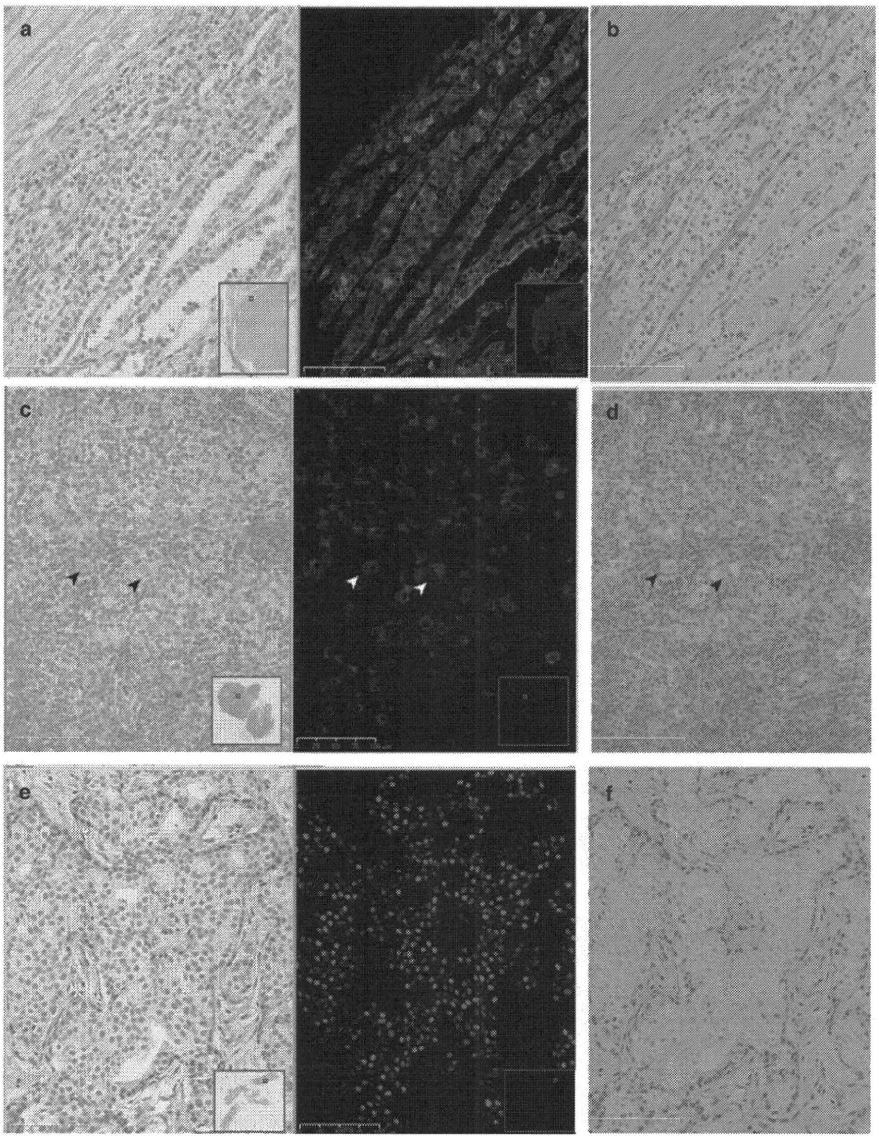

Figure 3 Screen shots of immunofluorescent quantification digital slides (IQD). Synchronized (**a,c,e**) and merged (**b,d,f**) viewing are indicated. In the former view, magnification changes and navigation in the samples are synchronized. In the bottom right-hand corner is an overview image with a marker indicating the current viewing position. (**a,b**) Chromogranin A in lung carcinoid tumors. (**c,d**) CD30 staining in the lymph node of Hodgkin's lymphoma. CD30 was positive for Reed-Sternberg cells (arrow heads). (**e,f**) Estrogen receptor in breast carcinomas.

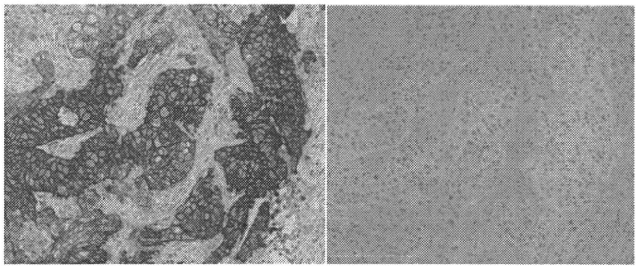

Figure 4 Comparison of immunofluorescent quantification digital slides (IQD) with immunohistochemistry (IHC) using serial sections. The human epidermal growth factor receptor 2 (HER2) staining in an invasive ductal carcinoma of the breast is shown. The IHC was classified as score 3+.

especially high in the formalin-fixed, paraffin-embedded tissue used widely in diagnostic pathology. On paraffin sections, strong and broad fluorescence of the section overlapping that of conventional fluorophores, such as fluorescein isothiocyanate (FITC), prevents detection of target antigens. This problem can be resolved using red-emitting quantum dots. A further problem is that long-term preservation of the immunofluorescence is all but impossible. In the last decade, advances in virtual microscopy enable us to scan the whole immunofluorescent slide image, and this technology may allow us to resolve this issue of preservation.

Immunofluorescent dyes (e.g. DAPI) are used to stain cell nuclei, although they may provide less morphological information than hematoxylin. In IQD pathologists may be able to easily identify cells by observing familiar hematoxilin-stained sections. We made IQD using two different methods, 'the one-step-scan' and 'the two-step-scan'. Hematoxylin staining before immunostaining and fluorescence scanning, did not affect the fluorescent signal of the membrane and cytoplasmic antigens we looked at. However, when using the one-step-scan method on other antigens it will be necessary to check for any effect of hematoxylin on immunostaining.

Table 1 The correlation between IQD and IHC scores, and comparing the groups classified by the IHC scores ($n = 30$)

	Differences in IQD score among IHC groups			Correlation between IQD and IHC scores	
	IHC score	IQD score	*P*-value	Correlation coefficient	*P*-value
HER2 score	1+	4 548 ± 1 951	0.02	0.509	<0.05
	2+	3 683 ± 1 735			
	3+	19 162 ± 10 426			
ERc	Negative	2 538 (1 589–3 007)	>0.05	0.523	<0.05
	Medium	2 420 (1 296–5 369)			
	High	3 830 (1 908–10 943)			
ER i	Negative	10 (8–16)	0.003	0.720	<0.001
	Medium	13 (10–45)			
	High	24.5 (14–82)			
PRc	Negative	2 173 ± 722	0.004	0.566	<0.05
	Medium	1 720 ± 305			
	High	3 667 ± 1 646			
PRi	Negative	10 (9–16)	0.01	0.705	<0.001
	Medium	11 (7–18)			
	High	24 (8–36)			

Mean ± SD, median (range).

ERc, estrogen receptor cell; ERi, estrogen receptor intensity index; IHC, immunohistochemistry; IQD, immunofluorescent quantification digital slides; PRc, progesterone receptor cell index; PRi, progesterone receptor intensity index.

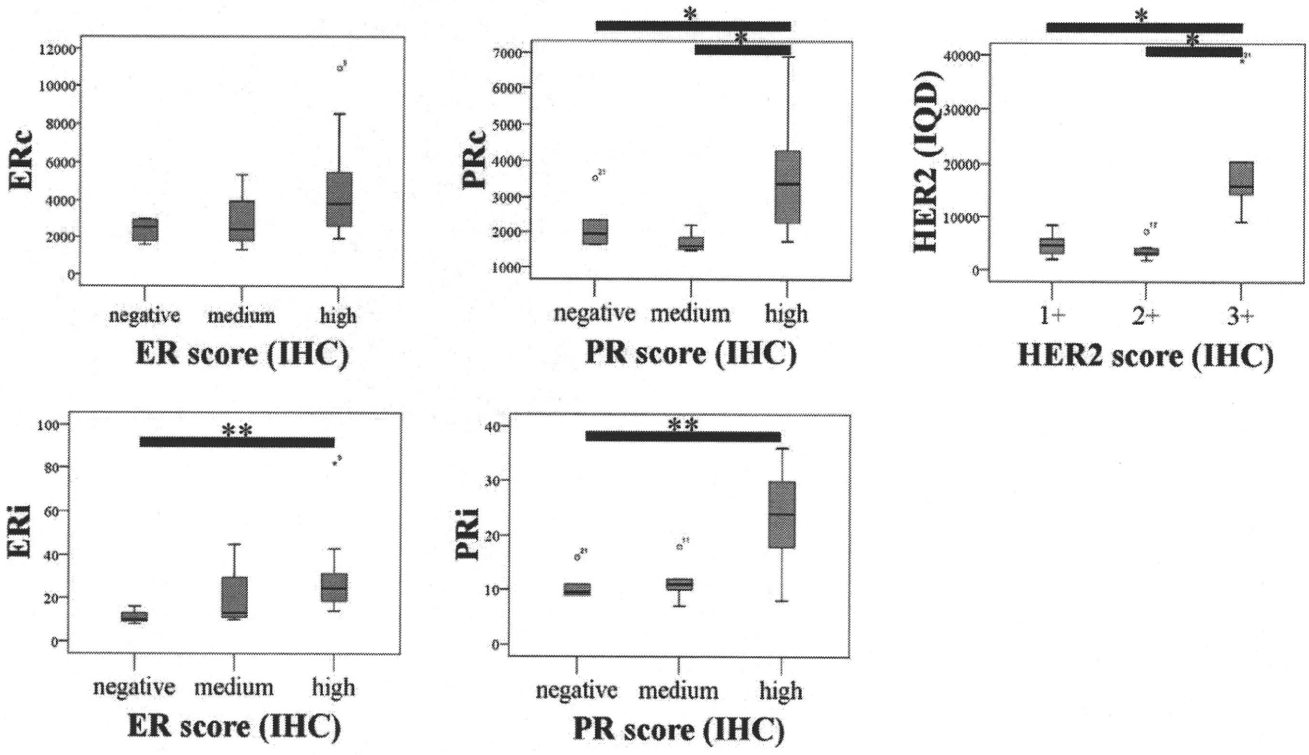

Figure 5 Box plots of immunofluorescent quantification digital slides (IQD) scores compared with immunohistochemistry (IHC). * Games-Howell test, $P < 0.05$, ** Mann-Whitney test, *P*-value < 0.017. ($n = 30$).

With the development of molecular targeted therapies for cancers, pathologists are requested to assess protein expression in tissue sections. We compared the quantitative data of IQD on HER2, and the simplified Allred score of IHC. When scoring in both IQD and IHC, the assessment area was selected by pathologists, to avoid selection bias. There were statistically significant correlations between the IQD and IHC scores. We also analyzed the difference in IQD scores among the IHC-scoring groups. We could not discriminate the IHC intermediate-expression group (e.g. ER and PR score 'medium' and HER2 score '2+') from the others (e.g. ER and PR score 'negative' and HER2 '1+'). This result may indicate

that the intermediate-expression group contains samples with a wide range of IQD scores. The IHC signals may be complicated due to enzymatic amplification, while the IQD cannot detect antigens of low-expression due to low sensitivity of indirect IF methods. We have shown the utility of IQD for diagnostic pathology, however, the clinical significance of IQD scores was not determined in this study. There are many problems associated with the use of IHC for evaluating biomarkers in diagnostic pathology, such as tissue fixation, the efficiency of the antigen retrieval, enzymatic amplification of the signal, and the scoring method.[3,12] Immunofluorescent staining is better than chromogenic staining for quantifying protein expression levels because a fluorescent signal has a wide dynamic range and is not modified by enzymatic amplification. The automated quantitative analysis (AQUA) system recently developed[13,14] demonstrates the advantage of immunofluorescent staining over IHC.[3,15,16] IQD may thus present a solution to the problems associated with IHC.

We have shown the utility of immunofluorescence in molecular assessment of tissue sections using digital technology and virtual microscopy. The IQD are not 'virtual' slides, but represent a novel diagnostic tool as there is no 'real' glass slide for the quantification of *in situ* protein expression. Immunofluorescent quantification digital slides may be a novel application of virtual microscopy, and can be applied, not only to diagnostic pathology, but also to research on molecular targets to diagnose and treat cancer.

ACKNOWLEDGMENTS

The authors thank K. Takeichi and M. Ohshiro for technical assistance. This study was supported in part by the New Energy and Industrial Technology Development Organization (NEDO).

REFERENCES

1 Yaziji H, Gown AM. Accuracy and precision in HER2/neu testing in breast cancer: Are we there yet? *Hum Pathol* 2004; **35**: 143–6.
2 Gown AM. Current issues in ER and HER2 testing by IHC in breast cancer. *Mod Pathol* 2008; **21** (Suppl. 2): S8–S15.
3 Rimm DL. What brown cannot do for you. *Nat Biotechnol* 2006; **24**: 914–16.
4 Weinstein RS, Graham AR, Richter LC *et al.* Overview of telepathology, virtual microscopy, and whole slide imaging: Prospects for the future. *Hum Pathol* 2009; **40**: 1057–69.
5 Krupinski EA. Virtual slide telepathology workstation of the future: Lessons learned from teleradiology. *Hum Pathol* 2009; **40**: 1100–11.
6 Dee FR. Virtual microscopy in pathology education. *Hum Pathol* 2009; **40**: 1112–21.
7 Helin HO, Lundin ME, Laakso M, Lundin J, Helin HJ, Isola J. Virtual microscopy in prostate histopathology: Simultaneous viewing of biopsies stained sequentially with hematoxylin and eosin, and alpha-methylacyl-coenzyme A racemase/p63 immunohistochemistry. *J Urol* 2006; **175**: 495–9.
8 Fountaine TJ, Wincovitch SM, Geho DH, Garfield SH, Pittaluga S. Multispectral imaging of clinically relevant cellular targets in tonsil and lymphoid tissue using semiconductor quantum dots. *Mod Pathol* 2006; **19**: 1181–91.
9 Xu X, Gimotty PA, Guerry D *et al.* Lymphatic invasion revealed by multispectral imaging is common in primary melanomas and associates with prognosis. *Hum Pathol* 2008; **39**: 901–9.
10 Wolff AC, Hammond ME, Schwartz JN *et al.* American Society of Clinical Oncology/College of American Pathologists guideline recommendations for human epidermal growth factor receptor 2 testing in breast cancer. *Arch Pathol Lab Med* 2007; **131**: 18–43.
11 Allred DC, Harvey JM, Berardo M, Clark GM. Prognostic and predictive factors in breast cancer by immunohistochemical analysis. *Mod Pathol* 1998; **11**: 155–68.
12 Wasielewski R, Hasselmann S, Ruschoff J, Fisseler-Eckhoff A, Kreipe H. Proficiency testing of immunohistochemical biomarker assays in breast cancer. *Virchows Arch* 2008; **453**: 537–43.
13 Camp RL, Chung GG, Rimm DL. Automated subcellular localization and quantification of protein expression in tissue microarrays. *Nat Med* 2002; **8**: 1323–7.
14 Camp RL, Dolled-Filhart M, King BL, Rimm DL. Quantitative analysis of breast cancer tissue microarrays shows that both high and normal levels of HER2 expression are associated with poor outcome. *Cancer Res* 2003; **63**: 1445–8.
15 Chung GG, Zerkowski MP, Ghosh S, Camp RL, Rimm DL. Quantitative analysis of estrogen receptor heterogeneity in breast cancer. *Lab Invest* 2007; **87**: 662–9.
16 Giltnane JM, Molinaro A, Cheng H *et al.* Comparison of quantitative immunofluorescence with conventional methods for HER2/neu testing with respect to response to trastuzumab therapy in metastatic breast cancer. *Arch Pathol Lab Med* 2008; **132**: 1635–47.